THE JOURNAL OF PHYSICAL CHEMISTRY B

ARTICLE

pubs.acs.org/JPCB

Kinetics and Mechanism of *S*-Nitrosothiol Acid-Catalyzed Hydrolysis: Sulfur Activation Promotes Facile NO^+ Release

Ernesto E. Moran,[†] Qadir K. Timerghazin,[*,†,§] Elizabeth Kwong,[‡] and Ann M. English[*,†]

[†]Department of Chemistry and Biochemistry and Centre for Research in Molecular Modeling, Concordia University, Montreal, Québec H3G 1M8, Canada

[‡]Pharmaceutical Research and Development, Merck Frosst Canada Incorporated, Kirkland, Québec H9H 3L1, Canada

Supporting Information

ABSTRACT: The denitrosation of three primary *S*-nitrosothiols (RSNO; *S*-nitrosocysteine, *S*-nitroso-*N*-acetylcysteine, and *S*-nitrosoglutathione) and two tertiary RSNOs (*S*-nitrosopenicillamine and *S*-nitroso-*N*-acetylpenicillamine) was investigated in 3.75 M H_2SO_4 to probe the mechanism of acid-catalyzed RSNO hydrolysis and its dependence on RSNO structure. This reversible reaction was forced to proceed in the denitrosation direction by trapping the nitrosating agent with HN_3. The primary RSNOs exhibited hydrolysis k_{obs} values of $\sim 2 \times 10^{-4}$ s^{-1}, and the tertiary RSNO k_{obs} values were an order of magnitude higher. Product analysis by HPLC revealed that the parent thiols (RSHs) were formed in 90−100% yield on 79−99% RSNO denitrosation. Possible hydrolysis mechanisms were studied computationally at the CBS-QB3 level using *S*-nitrosomethanethiol (MeSNO) as a model RSNO. Consideration of RSNOs as a combination of conventional R−S−N=O, zwitterionic $R-S^+=N-O^-$, and RS^-/NO^+ ion-pair resonance structures was key in understanding the mechanistic details of acid-catalyzed hydrolysis. Protonation of the *S*-nitroso oxygen or nitrogen activates the sulfur and nucleophilic attack by H_2O at this atom leads to the formation of the sulfoxide-protonated *N*-hydroxysulfinamide, $MeS^+(OH)NHOH$, with barriers of 19 and 29 kcal/mol, respectively. Proton loss and reprotonation at the nitrogen lead to secondary hydrolysis that produces the sulfinic acid MeS(=O)OH and NH_2OH. Notably, no low-energy RSNO hydrolysis pathway for HNO release was found in the computational analysis. Protonation of the *S*-nitroso sulfur gives rise to NO^+ release with a low activation barrier ($\Delta H^{\ddagger}_{calc} \approx 6$ kcal/mol) and the formation of MeSH in agreement with experiment. The experimental k_{obs} can be expressed as $K_a k_1$, where K_a is the acid dissociation constant for protonation of the *S*-nitroso sulfur and k_1 the pseudo-first-order hydrolysis rate constant. Given the low $\Delta H^{\ddagger}_{calc}$ for denitrosation of the *S*-protonated isomer, the observed slow rates of acid-catalyzed RSNO hydrolysis must be controlled by the magnitude of K_a. The 10-fold higher K_a calculated for $Me_3CS(H^+)NO$ ($\sim 10^{-15}$) compared to $MeS(H^+)NO$ (10^{-16}) is consistent with the order of magnitude larger k_{obs} reported here for the tertiary vs primary RSNOs.

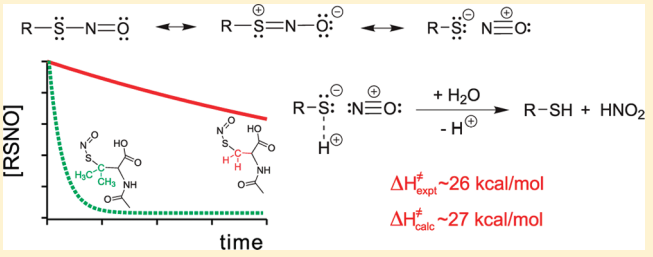

INTRODUCTION

Nitric oxide (NO) is an important molecule in mammalian physiology that is synthesized in vivo by the action of NO synthases.[1] It is a key player in biological processes such as vasodilation, the immune response, and neuronal signaling,[2] and similar physiological functions have been attributed to nitroxyl (HNO), the one-electron-reduced form of NO.[3] *S*-Nitrosothiols (RSNOs) are believed to act as NO transporters in vivo and are routinely used as donors of NO bioactivity[4] and may also function as HNO donors.[5,6] Notably, GSNO, which is the product of *S*-nitrosation of the abundant intracellular antioxidant, glutathione, has been detected in vivo.[7−9] However, pathways that release NO bioactivity vs HNO have been poorly explored and warrant further investigation given the reported distinct pharmacology of established HNO and NO donors.[10]

Hydrolysis of the S−NO bond following nucleophilic attack by water on both the *S*-nitroso nitrogen and the sulfur atoms has been proposed[5,6]

$$RSNO + H_2O \rightleftharpoons RSH + HNO_2 \quad (1)$$

$$RSNO + H_2O \rightleftharpoons RSOH + HNO \quad (2)$$

However, despite the potential importance of RSNO hydrolysis in vivo, the products remain poorly defined. Since the equilibrium in eq 1 lies strongly to the left, addition of a HNO_2 trap is necessary to study denitrosation in vitro. Williams and co-workers used high acidity (1−4 M H_2SO_4) and HN_3 (added as NaN_3; pK_a HN_3 = 4.72[11]) to trap the nitrosating agent(s) and promote hydrolysis of the stable RSNO, (±)-2-acetylamino-2-carboxy-1,1-dimethylethanethiol (or *S*-nitroso-*N*-acetylpenicillamine, SNAP, **5**).[12] They observed that SNAP hydrolysis is strongly acid catalyzed, and nucleophiles such as Cl^-, Br^-, and SCN^- were found to accelerate hydrolysis in a concentration-dependent manner.[12]

Received: April 20, 2010
Revised: January 21, 2011
Published: March 08, 2011

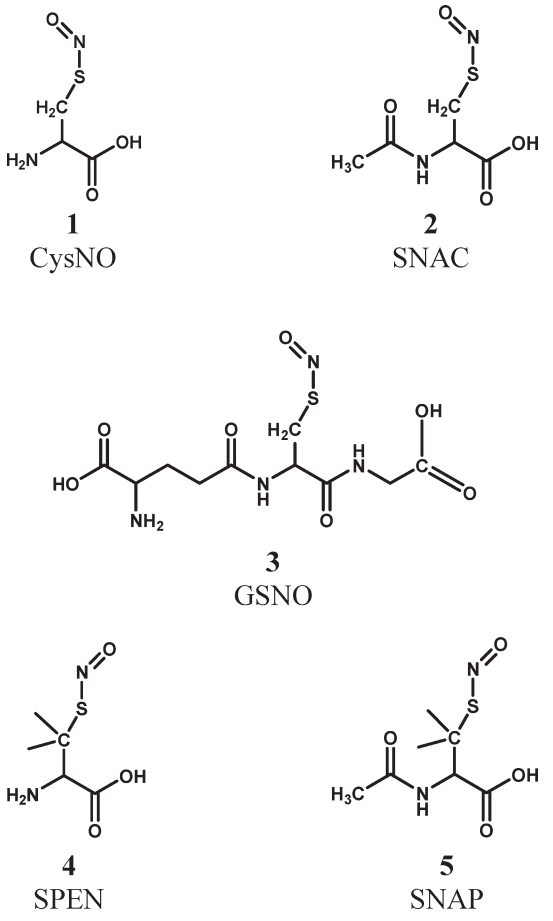

Figure 1. Structural formulas of the *S*-nitrosothiols investigated: **1** *S*-nitrosocysteine (CysNO), **2** *S*-nitroso-*N*-acetylated-cysteine (SNAC), **3** *S*-nitrosoglutathione (GSNO), **4** *S*-nitrosopenicillamine (SPEN), and **5** *S*-nitroso-*N*-acetylated-penicillamine (SNAP).

An unstable product with the same UV spectrum as the parent RSH, *N*-acetylpenicillamine (NAP), was detected, but no yield was reported.[12] Surprisingly, product instability was attributed to sulfhydryl oxidation, although low pH dramatically slows down RSH oxidation.[13]

Since we previously proposed[14] RSNO denitrosation via reaction 2, we interpreted the reported product instability[12] as further evidence for the competing formation of NAP sulfenic acid (RSOH). Sulfenic acids are highly unstable[15,16] and would likely react with any RSH produced. Also, our observation of strong inhibition of *S*-nitrosoglutathione (GSNO, **3**) denitrosation in water at pH ≈ 4 by the sulfenic acid trap, dimedone, supported this hypothesis, but product analysis was not performed in our previous study.[14] Clearly, quantitation of the denitrosated products is necessary to establish the pathway(s) of RSNO hydrolysis, and a HPLC−UV method was used here for this purpose. The hydrolysis reactions selected for analysis were those of three primary and two tertiary cysteine-derived RSNOs (Figure 1) of biological and pharmacological importance: *S*-nitrosocysteine (CysNO, **1**), *S*-nitroso-*N*-acetylcysteine (SNAC, **2**), GSNO (**3**), *S*-nitrosopenicillamine (SPEN, **4**), and SNAP (**5**).

To better understand the intrinsic reactivities of RSNOs and to elucidate the reaction mechanism, we carried out a detailed systematic computational analysis of MeSNO hydrolysis. Recently, we have shown computationally that the electronic structure of RSNOs can be described as a combination of three resonance structures.[17] These structures, shown in eq 3 with their relative weights estimated from natural resonance theory (NRT),[18] include the conventional form ***S***, a zwitterionic form ***D*** (where the labels emphasize the presence of a single and double S−N bond, respectively), plus an ionic form ***I***

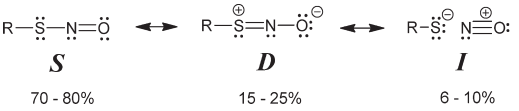

(3)

This resonance representation successfully rationalizes some of the seeming contradictory structural properties and the stability of RSNOs as discussed in our previous work.[17] Briefly, the weak bond dissociation energy ($D_e \approx 30$ kcal/mol) and elongated (∼1.8 Å) S−N bond[19,20] result from the contribution of the ionic resonance structure ***I***, whereas the partial double-bond character of the S−N bond, as reflected in the existence of cis and trans conformers, arises from the zwitterionic structure ***D***.[17] Importantly, the resonance description reveals that the reactivity of the *S*-nitroso group toward nucleophiles can be controlled by changing the relative contributions of ***D*** and ***I*** since this controls the electrophilicity of the sulfur and nitrogen atoms. Here, we use resonance theory to interpret the results of quantum chemistry analysis of the reaction pathways for uncatalyzed and acid-catalyzed MeSNO hydrolysis.

EXPERIMENTAL SECTION

Materials. All reagents were purchased from Sigma-Aldrich (St. Louis, MO), with the exception of diethylenetriaminepentaacetic acid (DTPA), which was from Koch-Light Laboratories (Colnbrook, Bucks, U.K.). The primary RSHs were directly dissolved in 125 mM aqueous H_2SO_4, while the tertiary RSHs were dissolved in MeOH and then diluted into 125 mM aqueous H_2SO_4 with 2.5% MeOH. Stock 10 mM RSNO solutions were prepared in situ by mixing equal volumes of 20 mM RSH in 125 mM H_2SO_4 with 20 mM $NaNO_2$ in 2 mM aqueous DTPA (to inhibit metal ion catalysis of RSNO decomposition), followed by a 10 min incubation period at room temperature in the dark.[21,22] HPLC analysis (described below) revealed 100% RSNO formation since no RSH was detected in the samples. The stock RSNO solutions were prepared on the day of the experiment and kept on ice before use.

Methods. *Hydrolysis Reactions.* The denitrosation reactions were followed spectrophotometrically on a model 8453 diode-array UV−vis spectrophotometer equipped with a thermostatted cell holder (Agilent Technologies, Santa Clara, CA). To minimize RSNO photodegradation, the solutions were protected from light throughout the experiments. The open spectrophotometer cell holder was also shielded from the light, and the integration time was set to 0.1 s. At this setting, each reading resulted in ≤0.03% absorbance loss due to photolysis of the S−NO bond in the beam.[23] The hydrolysis reactions were conducted in duplicate. A 375 μL aliquot of 0−30 mM aqueous NaN_3 in 5.0 M H_2SO_4 (HNO_2 trap) was equilibrated in a sealed 700 μL semimicro quartz cell (1 cm path length) at the desired temperature for 5 min in the spectrophotometer cell holder. A 50 μL aliquot of 10 mM RSNO stock was added, the sample was diluted to 500 μL to give a final [RSNO] of 1.0 mM in 3.75 M aqueous H_2SO_4 with 0.1 mM DTPA, and the cuvettes were tightly sealed to prevent loss of HN_3. After the spectra were

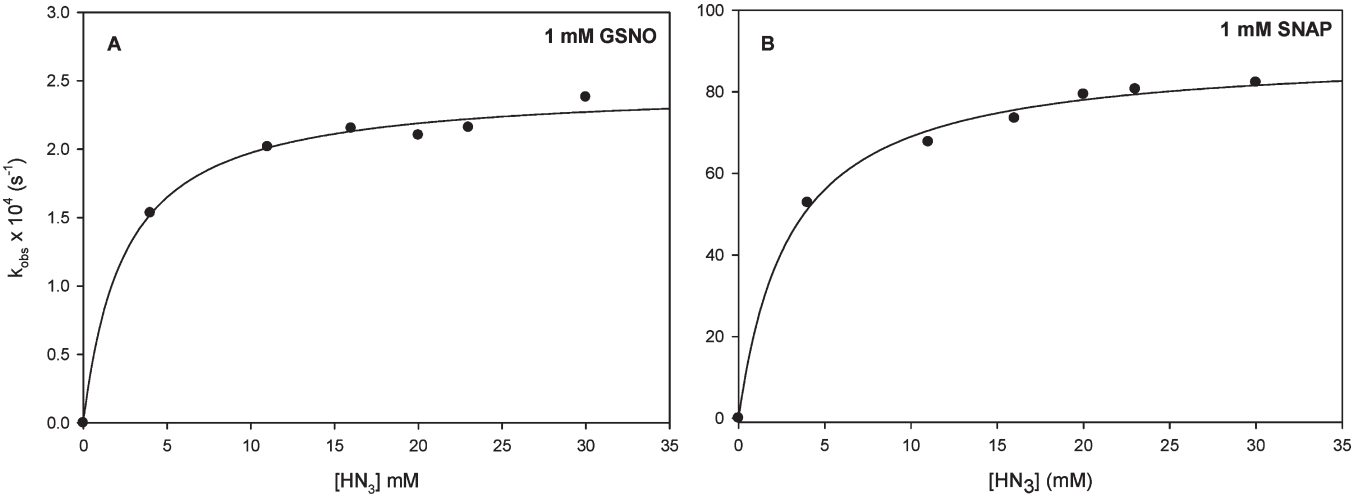

Figure 2. RSNO hydrolysis rate constants vs [HN_3]. Denitrosation of (A) 1.0 mM GSNO was monitored at 335 nm over 3 h, and (B) 1.0 mM SNAP was monitored at 338 nm over 15 min in 3.75 M aqueous H_2SO_4 with the indicated [HN_3] to trap the nitrosating species released on RSNO hydrolysis. HN_3 was formed in situ in the strongly acidic solutions on NaN_3 addition. The reaction solutions, which were shielded from light, also contained 0.1 mM DTPA; the SNAP solution additionally contained 2.5% v/v MeOH. Absorbances (Abs) were measured in a 1 cm cuvette at 31 °C with a 0.1 s integration time, and the k_{obs} values (dark circles) were calculated from plots of ln(Abs) vs time. The solid lines, which show rate saturation at high [HN_3], were generated by the curve-fitting algorithm in the SigmaPlot graphing program.

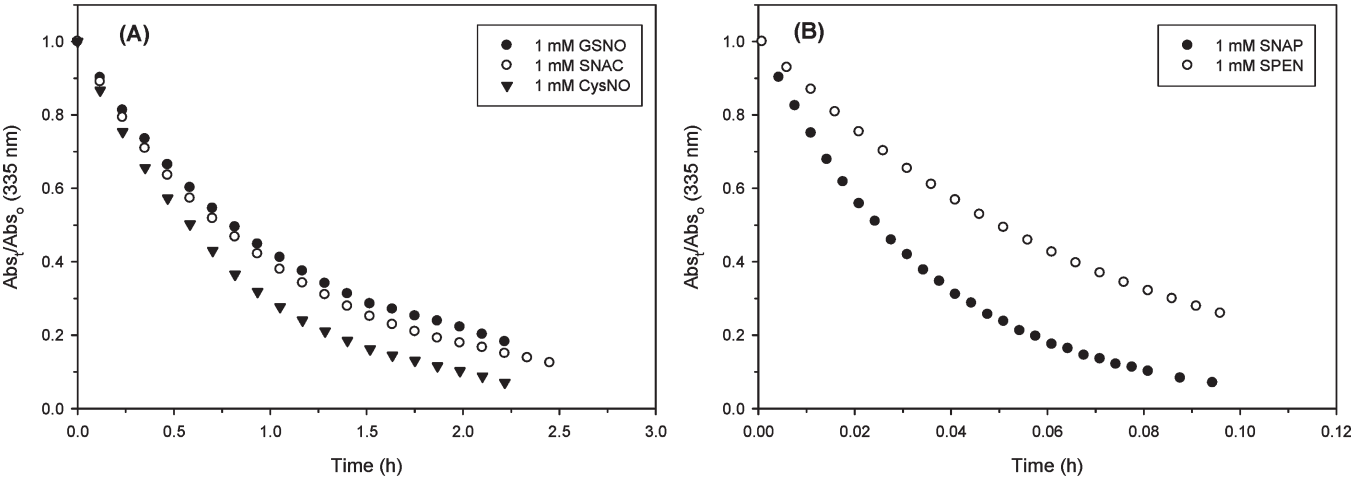

Figure 3. RSNO hydrolysis vs time. Plots of Abs_t/Abs_0 for (A) 1.0 mM GSNO, CysNO, and SNAC hydrolysis monitored at 335 nm and (B) 1.0 mM SNAP and SPEN monitored at 338 nm show exponential decay vs time. The reaction conditions are given in the legend to Figure 2.

corrected for background drift by subtracting the absorbance in the 800−830 nm region from each sample, denitrosation of the primary and tertiary RSNOs was monitored at 335 and 338 nm, respectively. A total of 20−30 absorbance readings were recorded during each experiment. The temperature dependence of primary (SNAC, **2**) and tertiary (SPEN, **4**) RSNO hydrolysis was compared below the bp (37 °C) of HN_3.

Products were analyzed by HPLC−UV using a model 1100 HPLC (Agilent Technologies, Santa Clara, CA) equipped with a variable wavelength detector set at 210 nm and controlled by ChemStation software, which was also used for analysis of the HPLC data. A 400 μL aliquot of the reaction solution was transferred into a 2 mL amber glass HPLC vial (Agilent Technologies, Santa Clara, CA), the solution pH was adjusted to 6.0 by addition of 440 μL of 8.0 M NaOH, and the sample was injected immediately onto an Atlantis dC18 analytical HPLC column (150 × 3.0 mm, 5 μm particles, Waters Corp., Milford, MA) and eluted as described in the legend of Figure 5. Since qualitative HPLC analysis revealed that the parent RSH was the main product of RSNO hydrolysis, the peak area at 210 nm vs concentration was examined between 0.50 and 1.2 mM RSH. The response was found to be linear for each RSH (data not shown, and product yields were determined by HPLC by comparing the peak area of the test (product) solution to that of the corresponding freshly prepared 1.0 mM RSH standard.

Quantum-Chemistry Calculations. The CBS-QB3 composite methodology of Petersson and co-workers[24−26] as implemented in the Gaussian 03 suite of programs[27] was used throughout this work. The calculated properties of RSNOs are highly dependent on the basis set used, which necessitates extrapolation to the complete basis set limit (CBS).[28] Due to the multireference character of the RSNO wave function,[28,29] inclusion of electron correlation effects employing the coupled-cluster method with at least single, double, and perturbative triple excitations [CCSD(T)] is also necessary.[28] CBS-QB3 methodology relies on geometries optimized with the B3LYP hybrid density functional,[30−32]

dx.doi.org/10.1021/jp1035597 |J. Phys. Chem. B 2011, 115, 3112–3126

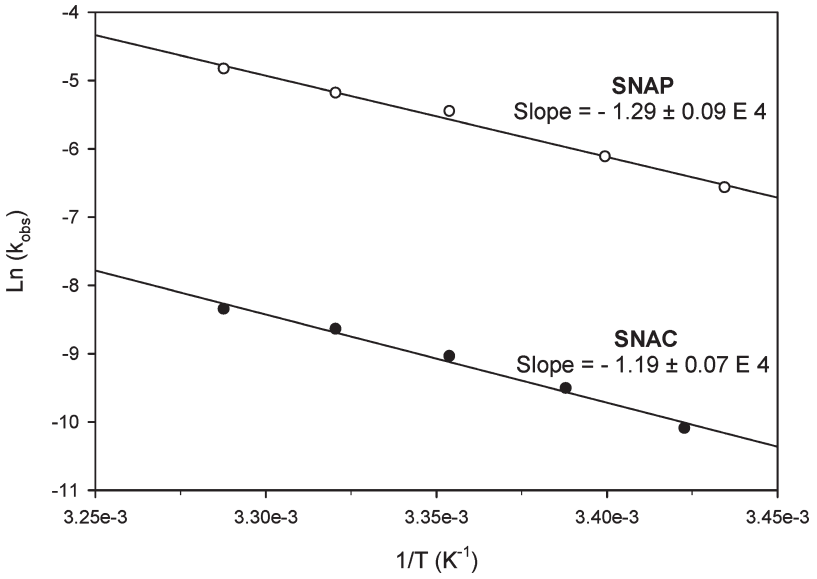

Figure 4. Temperature dependence of k_{obs} for SNAP and SNAC hydrolysis: (●) SNAC and (○) SNAP. Hydrolysis reactions were monitored at 18−31 °C as described in the legend to Figure 2. k_{obs} values were calculated from plots of ln(Abs) vs time. The solid line is the linear regression performed using the SigmaPlot graphing program.

Table 1. Temperature Dependence of RSNO Hydrolysis in 3.75 M Aqueous H_2SO_4 in the Dark[a]

RSNO	temp (°C)	$k_{obs} \times 10^4$ (s^{-1})[b]	E_a (kcal/mol)[c] [$\Delta H^{\ddagger}_{obs}$ (kcal/mol)]	A (s^{-1})[c] [$\Delta S^{\ddagger}_{obs}$ (kcal/mol/K)]
GSNO (1°)	31	2.10 ± 0.04		
CysNO (1°)	31	3.23 ± 0.03		
SNAC (1°)	31	2.35 ± 0.03	26 [26]	7.05×10^{14} [7.4]
	28	1.75 ± 0.01		
	25	1.18 ± 0.02		
	22	0.74 ± 0.01		
	19	0.41 ± 0.01		
SPEN (3°)	31	39.5 ± 0.1		
SNAP (3°)	31	79.4 ± 0.3 (81.7)[d]	23.7 [22.8]	7.81×10^{14} [5]
	28	55.8 ± 0.4		
	25	42.7 ± 0.4		
	21	22.0 ± 0.1		
	18	15.0 ± 0.1		

[a] Solutions in sealed cuvettes contained 1.0 mM primary (1°) or tertiary (3°) RSNO, 3.75 M H_2SO_4, 0.1 mM DTPA, and 20 mM HN_3 as a trap of the nitrosating agents. The SPEN and SNAP solutions additionally contained 2.5% v/v MeOH. [b] Calculated from plots of ln(Abs) vs time such as those shown in Figure 3. [c] Calculated from the slopes and intercepts of the regression lines of plots of $\ln(k_{obs})$ vs $1/T$ (Figure 4). [d] Value of k_{obs} reported by Williams and co-workers[12] at 31 °C in 3.77 M H_2SO_4.

which overestimates S−NO bond lengths in RSNOs by 0.02−0.1 Å depending on the basis set.[20,28] However, inclusion of the approximate CBS extrapolation[33] and the CCSD(T) correction renders the CBS-QB3 approach well suited for the study of RSNO reactions.[34,35]

Effects of the aqueous solvent were estimated by calculating free energies of solvation using the conductor-like polarizable continuum model (CPCM)[36,37] and single-point calculations at the B3LYP/6-311G(2d,d,p) level[24] for the gas-phase optimized geometries. The experimental value of −265.9 kcal/mol[38,39] was used for the proton solvation free energy $\Delta G_{solv}(H^+)$. Solution enthalpies were calculated as a sum of the solvation energies and the gas-phase CBS-QB3 enthalpies.[40] In the reaction profiles (Figures 6, 8, and 9, Supporting Information, Figures S1−S3), the enthalpies of the transition states (TSs), intermediates, and products in the gas and aqueous phases are relative to the sums of the enthalpies of the free reagents in the same phase.

Acidity constant (pK_a) values in aqueous solution were estimated following the protocol of Verdolino et al.[41] The gas-phase free energies were derived from the CBS-Q3 calculations, while the solvation free energies and solute distortion energies[41] were calculated at the B3LYP/6-311G(2d,d,p) level using the integral

dx.doi.org/10.1021/jp1035597 |J. Phys. Chem. B 2011, 115, 3112–3126

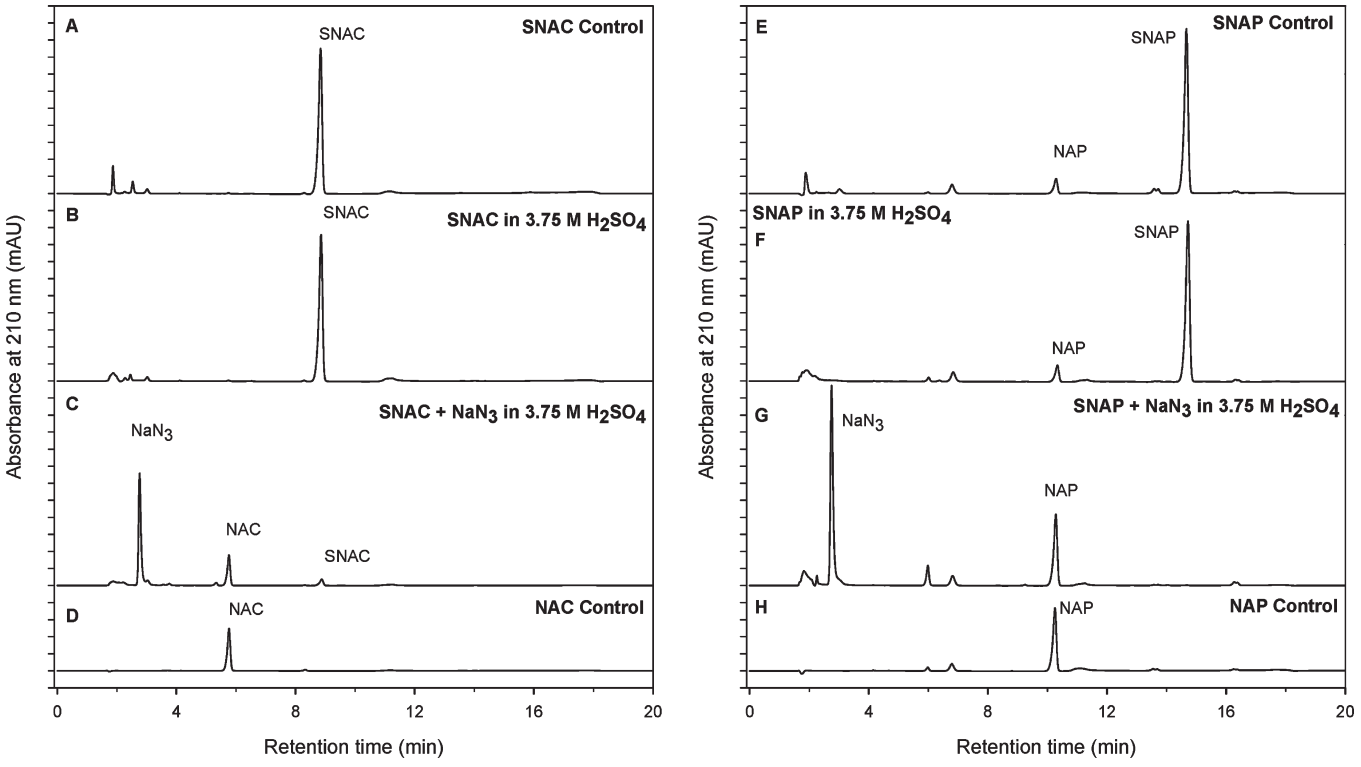

Figure 5. HPLC−UV analysis of SNAC and SNAP acid-catalyzed hydrolysis. Chromatograms following preincubation of the following: (A and E) RSNO controls, 1.0 mM SNAC or 1.0 mM SNAP in 50 mM sodium phosphate buffer (pH 2.0) for 3 h or 15 min, respectively; (B and F) 1.0 mM SNAC or 1.0 mM SNAP after 3 h or 15 min, respectively, in 3.75 M aqueous H_2SO_4; (C and G) 1.0 mM SNAC or 1.0 mM SNAP after 3 h or 15 min, respectively, in 3.75 M aqueous H_2SO_4 plus 20 mM HN_3 (HNO_2 trap); (D and H) RSH controls, 1.0 mM NAC or 1.0 mM NAP in 50 mM sodium phosphate buffer (pH 2.0) for 3 h or 15 min, respectively. The hydrolysis reaction conditions are given in the legend to Figure 2. Immediately prior to HPLC analysis, the reaction solutions in 3.75 M aqueous H_2SO_4 were adjusted to pH 6 by 2-fold dilution into 8 M aqueous NaOH to give the HPLC test solutions (B, C, F, and G) containing 0.50 mM RSX (RSNO, RSH) in 2 M Na_2SO_4, 0.5 mM NaCl, and 0.05 mM DTPA. The RSNO and RSH controls were also diluted to 0.50 mM with 50 mM sodium phosphate buffer (pH 2.0). The SNAP and NAP solutions additionally contained 1.3% v/v MeOH. An 80 mL aliquot of each solution was injected onto the C18 column equilibrated with 50 mM sodium phosphate buffer, pH 2.0 (mobile phase A) at 35 °C, and elution was performed at a flow rate of 1 mL/min with a gradient of 100% A to 100% B in 20 min followed by a 5 min isocratic hold at 100% B. Mobile phase B was 60% mobile phase A + 40% acetonitrile. The UV detector was set at 210 nm, and to facilitate the plotting of four chromatograms per panel, the absorbance readings (y axis) are presented on a continuous scale with each division representing 100 mAU. The chromatographic data, saved using the HPLC's ChemStation software, were plotted using SigmaPlot.

equation formalism polarizable continuum model (IEFPCM)[42] to include solvent effects. The 1 atm standard state in the gas phase was used in all calculations, except for the pK_a calculations where the 1 M solution standard state was used.

All geometries were fully optimized, and the energy minima and TSs were verified by vibrational frequency calculations. The chemical nature of each TS was also verified using intrinsic reaction coordinate calculations[43] to trace the reaction path from the TS to the reagents and products. Atomic charges were calculated using natural population analysis (NPA)[18] at the B3LYP/6-311G(2d,d,p) level. Some preliminary geometry calculations were performed at the PBE0/aug-pc-1 level.[44,45] Natural resonance theory (NRT)[18] analysis was also performed at the PBE0/aug-pc-1 level for consistency with our previous work.[17]

RESULTS

Trapping of the Nitrosating Agent(s) in 3.75 M Aqueous H_2SO_4. To examine RSNO hydrolysis it is necessary to trap any nitrosating agents to prevent RSH re-nitrosation.[12,22] Assuming attack solely at the *S*-nitroso nitrogen, Williams and co-workers[12] proposed the pathway in Scheme 1 for acid-catalyzed RSNO denitrosation, where Y is any nucleophile including H_2O.

In their analysis of 1.4 mM SNAP hydrolysis in 1−4 M H_2SO_4, the observed first-order rate constant, k_{obs}, was found to be independent of the $[HN_3]$ (trap) at 17 mM, signaling irreversible denitrosation ($k_2[HN_3] \gg k_{-1}[RSH]$).[12] Consistent with the published results,[12] Figure 2 shows that the observed constants (k_{obs}, s^{-1}) for denitrosation of both 1 mM GSNO and 1 mM SNAP in 3.75 M H_2SO_4 at 31 °C become independent of $[HN_3]$ around 20 mM, and 20 mM NaN_3 was added to form the trap in situ in the rest of the present study. Although the limiting k_{obs} for SNAP denitrosation is 38 times greater than that for GSNO (Table 1), their k_{obs} vs $[HN_3]$ profiles are similar indicating comparable *S*-nitrosation rates (i.e., $k_{-1}[RSH]$ values) when no trap is present, in agreement with published kinetic data (e.g., Table 18 of ref 22). Also based on published data (Table 4 of ref 46), a value of ~2 s^{-1} is predicted for the pseudo-first-order rate constant ($k_2[HN_3]$) for the trapping by 20 mM HN_3 of the nitrosating agent in strongly acidic media ($H_2NO_2^+$ or NO^+).[46,47] Since this value is 10^3−10^4-fold greater than the k_{obs} values for RSNO hydrolysis in Table 1 and the nitrosyl azide (N_3NO) trapping product rapidly (>10^6 s^{-1})[48] and irreversibly decomposes to N_2 and N_2O,[46] the trapping reaction can clearly be excluded from the rate-limiting step in hydrolysis.

dx.doi.org/10.1021/jp1035597 |*J. Phys. Chem. B* 2011, 115, 3112–3126

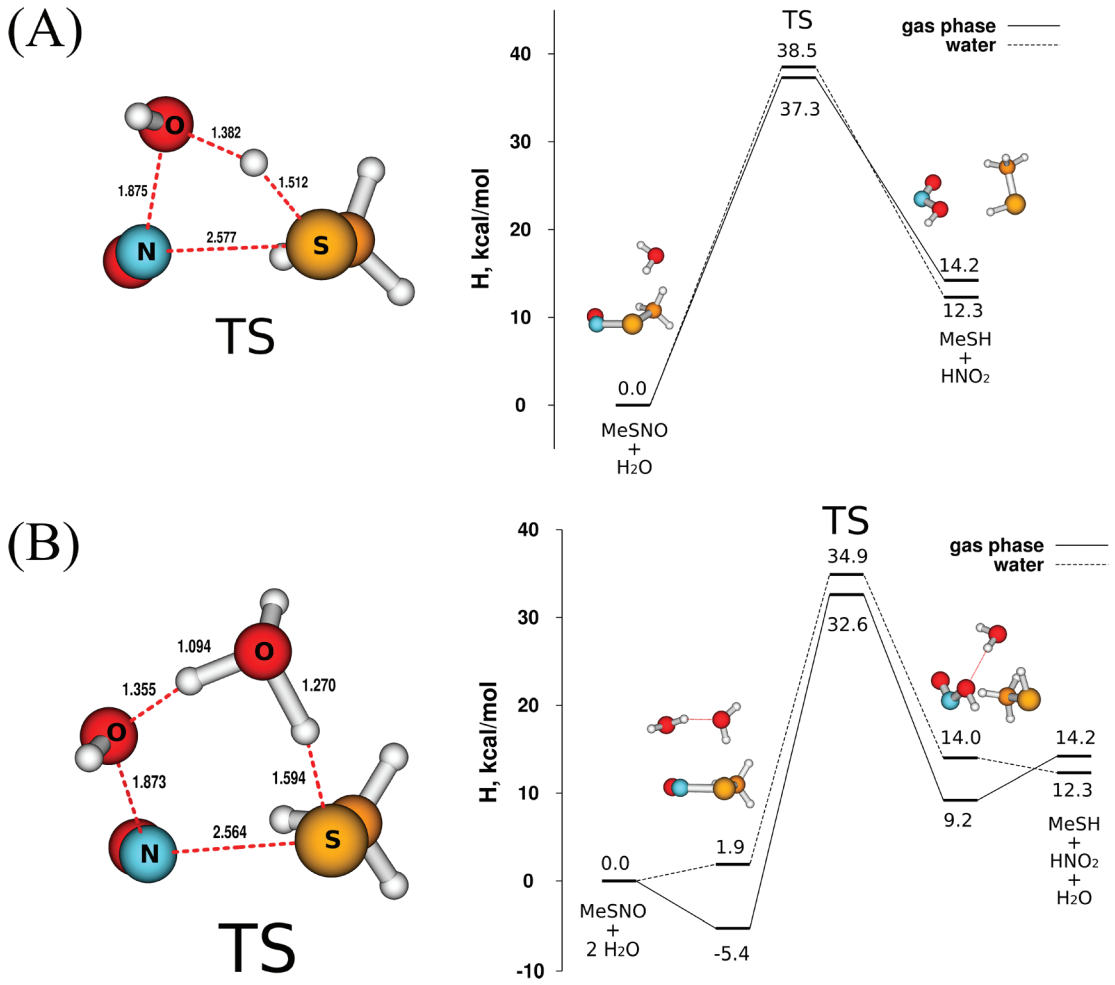

Figure 6. Modeling uncatalyzed attack at the nitrogen of MeSNO. Calculated structure of the transition state (TS) and enthalpy profile for the uncatalyzed hydrolysis of MeSNO following nucleophilic attack of (A) one and (B) two water molecules at the *S*-nitroso nitrogen atom. This yields MeSH and HNO_2 as products. Bond lengths are given in Angstroms (Å).

Scheme 1

$$RSNO + H^+ \rightleftharpoons RS(H^+)NO \underset{k_{-1}}{\overset{k_1,Y}{\rightleftharpoons}} RSH + NOY^+$$

$$NOY^+ + HN_3 \xrightarrow{k_2} N_2 + N_2O + Y + H^+$$

RSNO Hydrolysis in 3.75 M Aqueous H_2SO_4. The hydrolysis k_{obs} values ($\sim 2 \times 10^{-4}$ s^{-1}) for the three primary RSNOs, CysNO, SNAC, and GSNO, are very similar (Table 1 and Figure 3A). Notably, SNAC (i.e., *N*-acetylated CysNO, **2**) exhibits only a 1.4-fold slower hydrolysis rate than CysNO. Hence, substitution at the carbon β to the *S*-nitroso group has little effect on the RSNO hydrolysis rate in strongly acidic medium. Interestingly, the *N*-acetylated tertiary RSNO, SNAP (**5**) is hydrolyzed ~2-fold faster than SPEN (**4**) which possesses a free ammonium group in acidic media (Table 1 and Figure 3B). This divergent effect of *N*-acetylation on the hydrolysis rates mirrors that seen in the sulfhydryl pK_a values of the parent aminothiols: *N*-acetylation *raises* the pK_a(SH) of Cys (8.33) by ~1 pH unit but depresses that of penicillamine (11.08) by ~1 pH unit (English, A. Unpublished observations). This can be understood in terms of the relative values of pK_a(SH) and $pK_a(NH_3^+)$ for these aminothiols. For $pK_a(NH_3^+) > pK_a$(SH), as in Cys, *N*-acetylation increases pK_a(SH) but for $pK_a(NH_3^+) < pK_a$(SH), as in penicillamine, *N*-acetylation depresses pK_a(SH). However, the effect of *N*-actelyation on acid-catalyzed RSNO hydrolysis is small compared to its strong effect on sulfhydryl ionization in the aminothiols.

The dominant structural effect on RSNO hydrolysis in 3.75 M H_2SO_4 is that of the two methyl groups attached to the *S*-nitroso-bearing carbon in the tertiary RSNOs. The 34-fold higher hydrolysis rate of SNAP over SNAC (Table 1) is attributed to the inductive effect of the methyl groups, which facilitates sulfur protonation in the tertiary compared to the primary RSNOs (see below).

HPLC Analysis of the RSNO Hydrolysis Products. Product analysis was necessary to establish the mechanism(s) of RSNO hydrolysis, and the HPLC chromatograms of the SNAC and SNAP reaction products are shown in Figure 5. Note that in order to stack the chromatograms of the controls and samples, the absorbance readings (*y* axis) are presented on a continuous scale with each division representing 100 mAU in Figure 5. The peaks detected in the chromatograms following preincubation of 1.0 mM RSNO in 3.75 M aqueous H_2SO_4 without HN_3 (the trapping agent) and in 50 mM sodium phosphate buffer (pH 2.0)

dx.doi.org/10.1021/jp1035597 |*J. Phys. Chem. B* 2011, 115, 3112–3126

Table 2. Adjusted RSH Yields Following RSNO Hydrolysis in 3.75 M Aqueous H_2SO_4 in the Dark[a]

RSNO	initial [RSNO] (mM)	final [RSH][b] (mM)	% reaction (n)[c]	RSH yield[d] %
GSNO (1°)	1.0	0.71	79 (2.27)	90
CysNO (1°)	1.0	ND[e]	91 (3.49)	ND[e]
SNAC (1°)	1.0	0.82	83 (2.54)	99
SPEN (3°)	1.0	0.93	92 (3.56)	101
SNAP (3°)	1.0	0.91	99 (7.15)	92

[a] The reaction solutions (see footnote a in Table 1) were incubated at 31 °C for 3 h (1° RSNOs) or 15 min (3° RSNOs) in sealed cuvettes. [b] Calculated from the peak areas in the HPLC chromatograms. [c] The number of half-lives (n) were calculated from the k_{obs} (s^{-1}) values at 31 °C in Table 1 and the reaction times given in footnote a. The % reaction = $100(1 - 1/2^n)$. [d] RSH yields, which varied by ~1% between runs, are based on the initial [RSNO] and adjusted for the % reaction. [e] ND, not determined since cysteine was not retained by the HPLC column.

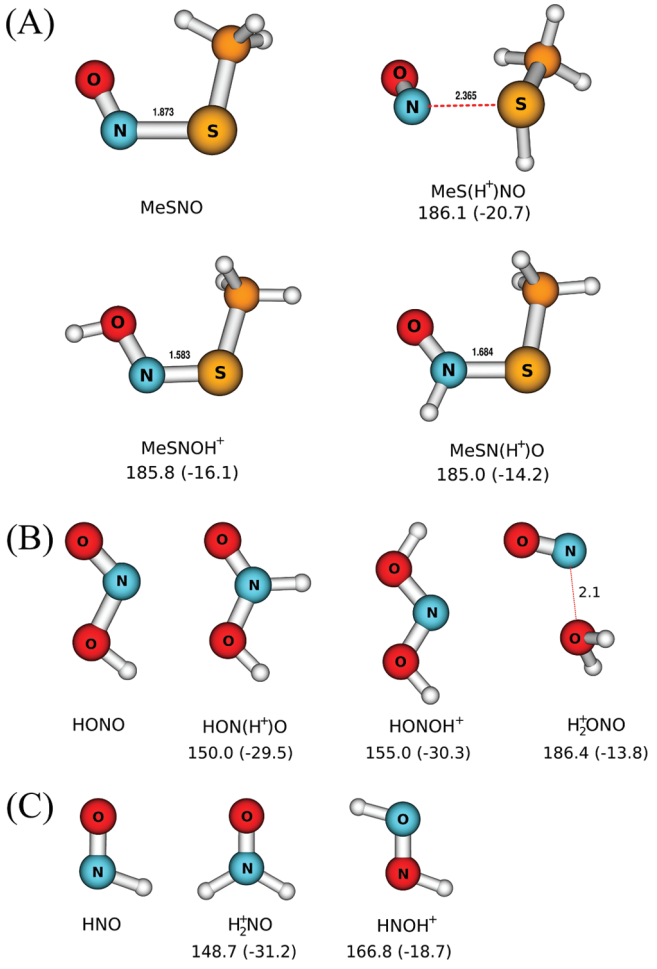

Figure 7. Protonated isomers of MeSNO, HNO_2, and HNO. Protonation of (A) MeSNO, (B) HNO_2, and (C) HNO and the corresponding proton affinities (PA) in kcal/mol. The values in parentheses ($PA + \Delta G_{solv}$) include the correction for solvation effects, ΔG_{solv}. Bond lengths are given in Angstroms (Å).

are the same (Figure 5A and 5E vs Figure 5B and 5F). This confirms that the RSNOs are stable to degradation in high acid and that the *N*-acetyl group of both SNAC and SNAP is preserved. Figure 5 also reveals that the main product of RSNO hydrolysis in the presence of the trapping agent (formed in situ from NaN_3) is the corresponding RSH (Figure 5C and Figure 5G vs 5D and 5H). RSH yields varied by ~1% over multiple runs; thus, as summarized in Table 2, correction for % reaction reveals that 83% denitrosation of SNAC and 92% denitrosation of SPEN yielded stoichiometric RSH within experimental error. RSH is the expected organic product following RSNO denitrosation by attack of water at the *S*-nitroso nitrogen when the nitrosating agent is trapped (eq 1 and Scheme 1).

RSH yields of 90% and 92% were obtained on 79% and 99% denitrosation of GSNO and SNAP, respectively (Table 2), indicating that attack at nitrogen is also the dominant hydrolysis pathway for these two RSNOs (eq 1). Attack at sulfur was predicted to yield the unstable products RSOH and HNO (eq 2)[6,12,14] that rapidly self-condense to RS(O)SR[15,16] (which further disproportionates to RSO_2SR and RSSR) and nitrous oxide (N_2O), respectively. If their reactions with RSH are similar in highly acidic solutions to those observed around physiological pH, both RSOH[49] and HNO[50] could, in competition with their self-condensation, oxidize RSH formed in situ to RSSR with the additional possibility of RSH oxidation to RS(=O)NH by HNO.[3] However, HNO generation on RSNO hydrolysis is not supported by the computational analysis of the reactions as discussed below. For example, GSNO denitrosation yielded substoichiometric GSH (Table 2), raising the possibility of GSSG formation. Thus, a solution of GSNO and GSSG was examined by HPLC under the conditions outlined in the legend to Figure 5. GSNO eluted at 6.48 min and GSSG at 5.65 min (data not shown), indicating that the disulfide has lower affinity for the C18 column as expected. Although a very weak peak that could be assigned to trace disulfide was detected at ~5.5 min in the HPLC chromatograms of the GSNO reaction products, this peak was also present in the chromatogram of the commercial GSH used to prepare GSNO (data not shown). Hence, HPLC analysis does not support GSSG formation during the 3 h denitrosation reaction examined here.

The chromatogram of the SNAP products (Figure 5G) exhibits a more intense peak at 6 min than any of the control chromatograms (Figure 5E, 5F, and 5H). This peak likely contains a minor (~8%), hydrophilic derivative of NAP since the major (92%) NAP product peak appears at 10 min. Given that GSH has a low retention time on the C18 column (~4 min, data not shown), a hydrophilic GSH derivative might have been masked by the strong NaN_3 peak at ~3 min or it might not have been retained on the C18 column. The results of the computational analysis discussed below provide further insight into the minor hydrolysis pathway as well as the expected identity of the more hydrophilic products of SNAP and GSNO hydrolysis.

Combined, the data in Table 2 reveal that attack at the *S*-nitroso nitrogen leading to RSH formation is the sole pathway of acid-catalyzed hydrolysis of SNAC (**2**) and SPEN (**4**) and the dominant pathway of GSNO (**3**) and SNAP (**5**) hydrolysis. Since cysteine was not retained on the column, its yield on CysNO (**1**)

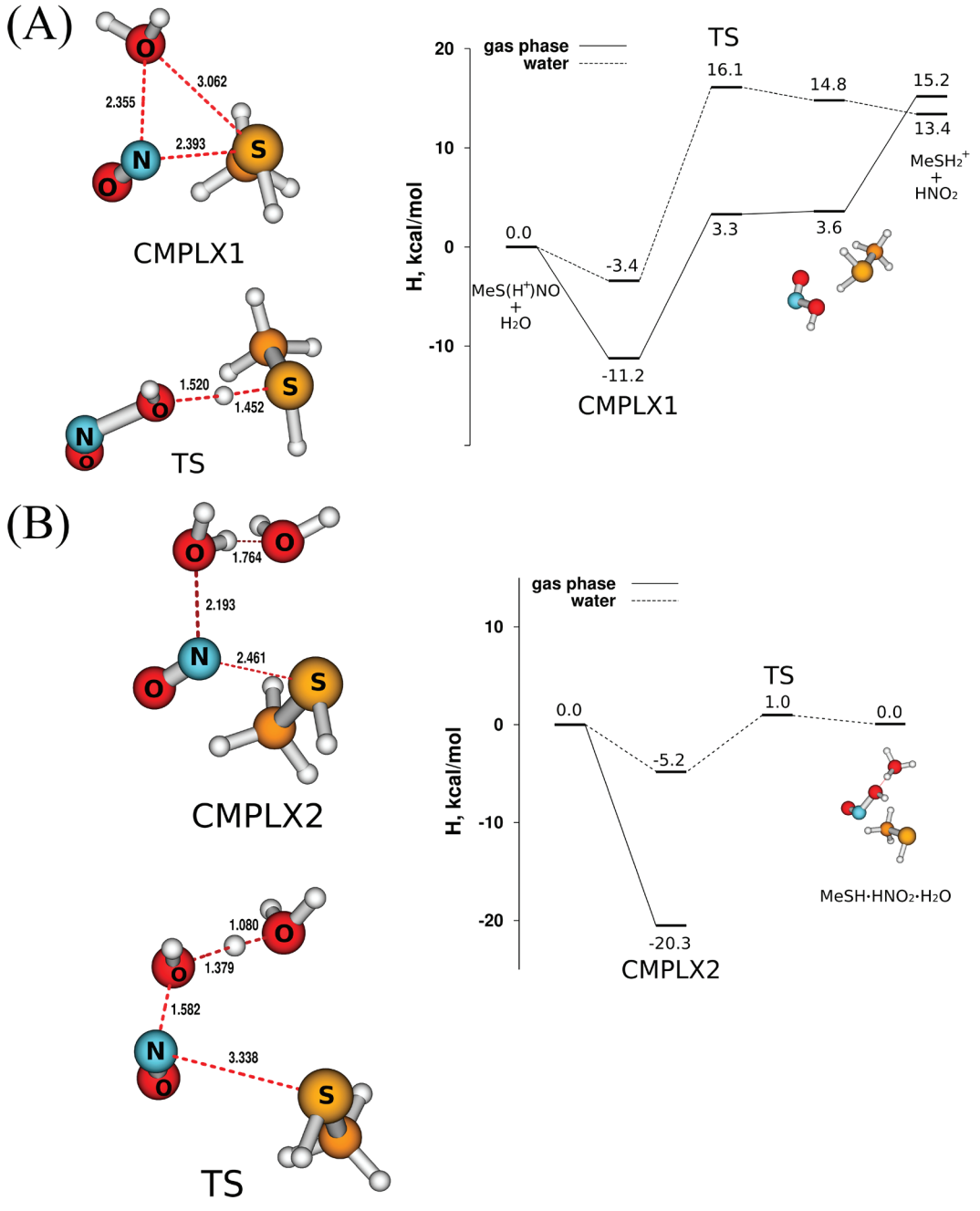

Figure 8. Modeling acid-catalyzed attack at the nitrogen of S-protonated MeSNO. Calculated structures of the prereactive complex (CMPLX), the transition state (TS), and the enthalpy profile for the acid-catalyzed hydrolysis of MeS(H^+)NO at the *S*-nitroso nitrogen atom with (A) one water molecule, which yields $MeSH_2^+$ and HNO_2 as products, and (B) two water molecules, which yields MeSH and HNO_2 as products. The TS and products in B were optimized in CPCM water since they could not be optimized in the gas phase. Bond lengths are given in Angstroms (Å).

hydrolysis could not be determined by HPLC. However, given its structural similarity to SNAC (Figure 1), as well as the similarity in their k_{obs} values (Table 1), we assume that CysNO hydrolysis also proceeds mainly via attack at the *S*-nitroso nitrogen.

Computational Study of Uncatalyzed MeSNO Hydrolysis. Since we report that *N*-acylation or *C*-terminal amidation has minor effects on the observed hydrolysis rates, substituents remote from the carbon bearing the *S*-nitroso group are unlikely to influence the reaction kinetics in highly acidic media. Thus, although MeSNO lacks the ionizable groups found in the RSNOs examined experimentally (**1**−**5**), it can be considered a good model for the theoretical studies while minimizing the required computational time.

The results of the computational modeling of uncatalyzed MeSNO hydrolysis are summarized in Table 3. Contribution from the MeS^- NO^+ ionic resonance structure ***I*** (eq 3) will strongly favor nucleophilic attack at the *S*-nitroso nitrogen.[17] Attack at nitrogen is also favored in the conventional resonance structure ***S*** since this atom possesses only one lone pair while the oxygen and sulfur atoms each have two lone pairs. The transition

dx.doi.org/10.1021/jp1035597 |*J. Phys. Chem. B* 2011, 115, 3112–3126

Table 3. Activation Enthalpies ($\Delta H^{\ddagger}_{calc}$) and Reaction Products Obtained in the Computational Modeling of MeSNO Hydrolysis

	$\Delta H^{\ddagger}_{calc}$ (kcal/mol)			
hydrolysis reaction[a]	gas phase	CPCM water	products	Figure
uncatalyzed				
Attack at N	38	33	MeSH + HNO_2	Figure 6B
Attack at S	52	47	MeSOH + HNO	Supporting Information Figure S1B
sulfur protonated				
Attack at N		6	MeSH + HNO_2 + H_3O^+	Figure 8B
oxygen protonated				
Attack at S	23	19	$MeS^+(OH)NHOH$[b]	Figure 9B
nitrogen protonated				
Attack at S	39	29	$MeS^+(OH)NHOH$[b]	Supporting Information Figure S2B
Attack at N	59	48	MeSH + HNO_2	Supporting Information Figure S2B

[a] Results for reactions modeled with a single water molecule are not tabulated (see text). [b] Sulfoxide-protonated *N*-hydroxysulfinamide, *N*-HSAH (see text, eqs 8 and 10 and Figure 9A).

state (TS) corresponding to water attack at nitrogen is characterized by simultaneous O−N bond formation and O−H bond cleavage (Figure 6A). It is a late TS since the S−N bond is highly elongated (2.58 Å) compared to that in the reactant (1.87 Å). The calculated activation barrier ($\Delta H^{\ddagger}_{calc}$) is 37.3 kcal/mol in the gas phase, and the products (MeSH + HNO_2) are 14.2 kcal/mol higher in enthalpy than the reactants (MeSNO + H_2O) (Figure 6A), in agreement with the equilibrium in eq 1 being strongly shifted toward RSNO formation in the absence of a HNO_2 trap. The $\Delta H^{\ddagger}_{calc}$ (38.5 kcal/mol) and product stability (12.3 kcal/mol) increase slightly with the inclusion of solvent (Figure 6A). As is typical of hydrolysis reactions, addition of a second water molecule allows concerted proton transfer, which lowers $\Delta H^{\ddagger}_{calc}$ to 33.0 kcal/mol in solvent (Figure 6B, Table 3).

Resonance structure ***D*** strongly favors attack at the sulfur atom, which is positively charged in this zwitterionic form (eq 3). However, attempts to locate the TS for uncatalyzed MeSNO hydrolysis involving nucleophilic attack of a single water molecule at the sulfur atom failed. Simultaneous solvent-assisted proton transfer to the nitrogen atom by a second water molecule did lead to a TS, but the gas-phase and solution $\Delta H^{\ddagger}_{calc}$ values are 52.2 and 46.9 kcal/mol, respectively (Table 3), and the products (MeSOH and HNO) are 26−30 kcal/mol less stable than the reactants (Supporting Information, Figure S1). Thus, uncatalyzed RSNO hydrolysis is expected to occur exclusively via water attack at the *S*-nitroso nitrogen. The calculations also expose the large deviation (∼0.7 Å) from the equilibrium S−N bond length (1.87 Å) required to activate the *S*-nitroso nitrogen toward attack by a weak nucleophile such as water (Figure 6). This reflects a change in the relative contribution of the resonance structures in eq 3 since NRT analysis[18] reveals that elongation of the S−N bond by ∼0.5 Å, for example, favors ***I*** (30%) over ***D*** (5%). The less favorable attack at the *S*-nitroso sulfur requires contraction of the S−N bond by 0.20 Å (Supporting Information, Figure S1), which would occur on doubling (15−30%) resonance structure ***D***'s contribution with loss of ***I***'s contribution (10−4%).

Computational Study of MeSNO, MeSH, HNO_2, and HNO Protonation. NRT[18] calculations reveal that ***I*** becomes the dominant resonance form of *S*-protonated MeSNO and ***D*** disappears[17]

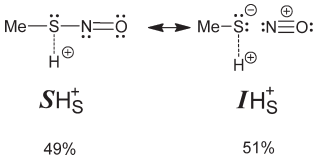

(4)

Atomic charge analysis indicates that the NO moiety carries a +0.5 charge, indicating that $MeS(H^+)NO$ can be partially considered as a complex of MeSH and NO^+, consistent with its highly elongated S−N bond (2.36 vs 1.87 Å in neutral MeSNO; Figure 7A).

O-Protonation strongly favors structure ***D*** with its negatively charged *S*-nitroso oxygen while ***I*** disappears[17]

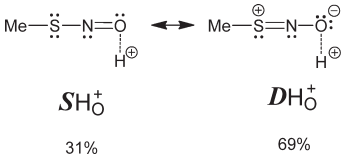

(5)

N-Protonation also favors ***D*** at the expense of ***I***

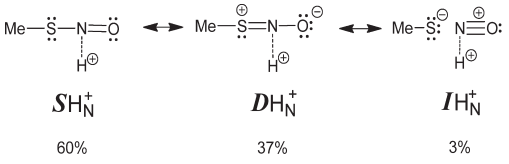

(6)

Stabilization of the S−N bond on O- or N-protonation leads to its contraction to 1.58 or 1.68 Å, respectively, from 1.87 Å in neutral MeSNO (Figure 7A). The calculated proton affinities (*PA*) of the MeSNO sulfur, oxygen, and nitrogen atoms are within 1 kcal/mol (Figure 7A), and their protonation in water is endothermic because the proton hydration energy is large, $\Delta G_{solv}(H^+) = -265.9$.[38,39] The ($PA + \Delta G_{solv}$) values reveal that $MeS(H^+)NO$ (−20.7 kcal/mol) is the least stable protonated isomer followed by $MeSNOH^+$ (−16.1 kcal/mol) and $MeSN(H^+)O$ (−14.2 kcal/mol) (Figure 7A).

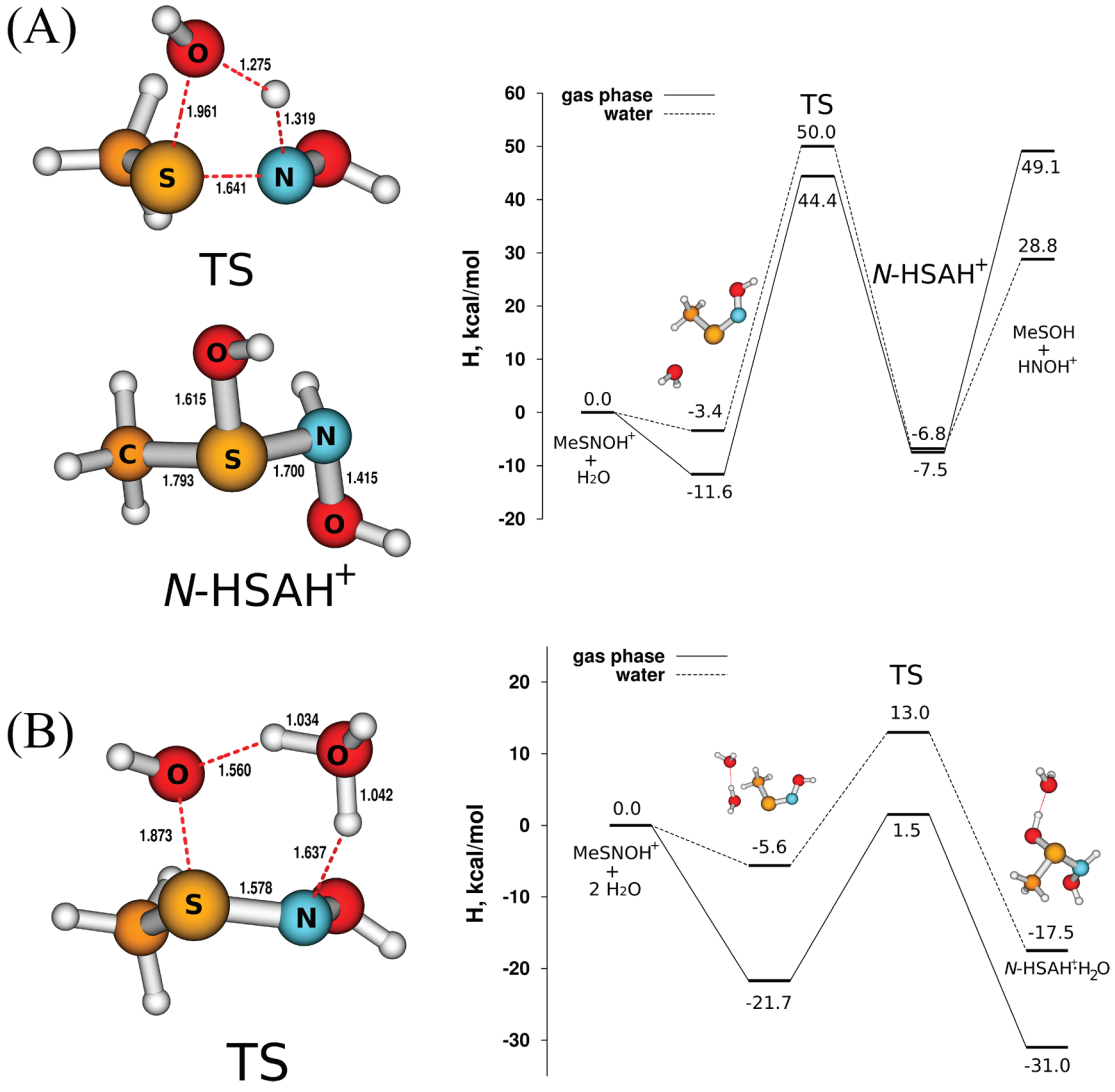

Figure 9. Modeling acid-catalyzed attack at the sulfur of O-protonated MeSNO. Calculated structure of the transition state (TS), the sulfoxide-protonated sulfonamide product, $MeS^{+}(OH)NHOH$ (*N*-HSAH^{+}), and the enthalpy profile for the acid-catalyzed hydrolysis of $MeSNOH^{+}$ at the *S*-nitroso sulfur atom with (A) one and (B) two water molecules. As can be seen from A, *N*-HSAH^{+} is stable to dissociation into MeSOH and H_2NO^{+}. Bond lengths are given in Angstroms (Å).

The structures and stabilities of the protonated forms of MeSH, HNO_2, and HNO were also examined to evaluate their involvement in acid-catalyzed RSNO hydrolysis. The calculated proton affinity of the MeSH sulfur is 185.1 kcal/mol, in excellent agreement with the experimental value of 184.8 kcal/mol,[51] and (PA + ΔG_{solv}) is −21.7 kcal/mol. In HNO_2, the hydroxyl oxygen possesses the highest proton affinity and protonation at this atom results in an unusually long N−O bond (∼2.1 Å, Figure 7B). Atomic charge analysis reveals a +0.8 charge on the NO moiety, indicating that this protonated isomer can be considered as a $H_2O\cdots NO^{+}$ complex. Solvation decreases the energy gap between the three $H_2NO_2^{+}$ isomers, but $H_2O\cdots NO^{+}$ remains ∼16 kcal/mol less endothermic, and hence more stable, than the other two isomers (Figure 7B). O-Protonation of HNO is more favorable than N-protonation by ∼18 and ∼12 kcal/mol in the gas phase and water, respectively (Figure 7C).

Computational Study of Acid-Catalyzed MeSNO Hydrolysis. *Sulfur Protonation.* S-Protonation leads to formation of a nascent $MeSH\cdots NO^{+}$ complex (eq 4) that renders the NO moiety highly susceptible to nucleophilic attack

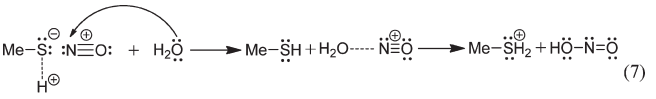

IH_S^{+}

The predicted prereaction complex with one water molecule (CMPLX1, Figure 8A) can be viewed as a termolecular complex of MeSH with $H_2O\cdots NO^{+}$, the most stable $H_2NO_2^{+}$ isomer (Figure 7B). Since $H_2O\cdots NO^{+}$ is also ∼7 kcal/mol more stable than $MeSH_2^{+}$, the protonated thiol is not an expected product following attack of H_2O on $MeS(H^{+})NO$. Indeed, proton transfer within CMPLX1 to yield $MeSH_2^{+}$ and HNO_2, which is the only way to form molecular HNO_2 in the presence of a single water molecule, is unfavorable and requires significant rearrangement with $\Delta H^{\ddagger}_{calc}$ values of 14.5 and 19.5 kcal/mol in

dx.doi.org/10.1021/jp1035597 |*J. Phys. Chem. B* 2011, 115, 3112–3126

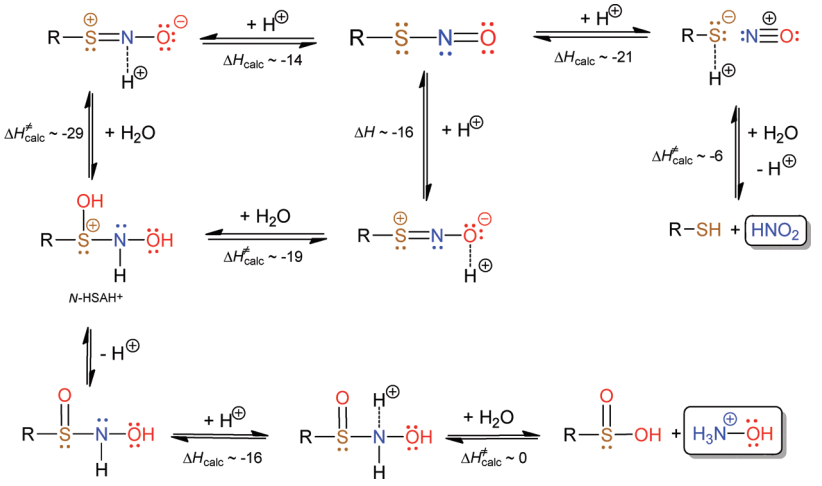

Figure 10. Main pathways and products of acid-catalyzed RSNO hydrolysis predicted by computational analysis. ΔH_{calc} and $\Delta H^{\ddagger}_{calc}$ values are expressed in kcal/mol (Table 3). Protonation of the *S*-nitroso sulfur (which yields the least stable protonated RSNO isomer, Figure 7A) promotes facile release and hydrolysis of NO^+ to HNO_2 with a low $\Delta H^{\ddagger}_{calc}$ (~6 kcal/mol) and RSH as the organic product (Figure 8B). Protonation of the *S*-nitroso oxygen or nitrogen yields a sulfoxide-protonated sulfinamide (*N*-HSAH$^+$) that readily undergoes deprotonation. N-Protonation of the resulting sulfinamide leads to barrierless NH_2OH release with the protonated sulfinic acid $RS(=O)OH_2^+$ as a coproduct (Supporting Information, Figure S4), and solvent-assisted proton transfer will yield NH_3OH^+ (pK_a 6.0) and RS(=O)OH. Hydrolysis of O-protonated $RSNOH^+$ (Figure 9B) is the preferred pathway to *N*-HSAH$^+$ ($\Delta H^{\ddagger}_{calc} \approx 19$ kcal/mol; Table 3). Also, from the data in Table 3, uncatalyzed RSNO hydrolysis (which is not depicted in this scheme) is expected to occur exclusively via attack on the *S*-nitroso nitrogen to produce RSH and HNO_2 (Figure 6B). Note that no low-energy pathway was found for *direct* HNO release from any of the protonated RSNO isomers or from unprotonated RSNO.

the gas phase and water, respectively (Figure 8A). The single-water reaction is discussed here only for completeness.

A prereaction complex (CMPLX2) with a second water hydrogen bonded to the $H_2O\cdots NO^+$ moiety is shown in Figure 8B. Proton transfer from $H_2O\cdots NO^+$ to the peripheral H_2O yields MeSH, HNO_2, and H_3O^+, and a TS for this process with $\Delta H^{\ddagger}_{calc} \approx 6$ kcal/mol was located in water using the CPCM solvent model but not in the gas phase (Table 3). This very late TS with an S−N separation of 3.34 Å is only ~1 kcal/mol higher in energy than the products. Thus, RSNO hydrolysis catalyzed by sulfur protonation most likely proceeds via formation of RSH and a nascent NO^+ cation with synchronous attack by water on NO^+ to generate $H_2NO_2^+$, which can donate a proton to the solvent.

Oxygen Protonation. O-Protonation favors resonance structure ***D*** (eq 5) and hence nucleophilic attack at the *S*-nitroso sulfur. A TS corresponding to simultaneous S−O bond formation and proton transfer from H_2O to the nitrogen was readily located in the reaction of $MeSNOH^+$ with a single water molecule (Figure 9A). However, $\Delta H^{\ddagger}_{calc}$ is high (56.0 and 53.4 kcal/mol in the gas phase and water, respectively), and the sulfoxide-protonated *N*-hydroxysulfinamide (*N*-HSAH$^+$, eq 8) is stable to dissociation to the predicted products (eq 2), MeSOH and H_2NO^+, by 55.9 and 36.3 kcal/mol in the gas phase and water, respectively (Figure 9A).

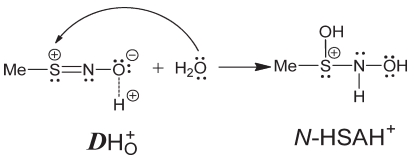

***D*H^+_O** *N*-HSAH$^+$ (8)

Introduction of a second water assists proton transfer to nitrogen in the TS, which dramatically decreases $\Delta H^{\ddagger}_{calc}$ to 23.2 kcal/mol in the gas phase and 18.6 kcal/mol in water (Table 3). However, again, simultaneous S−O bond formation leads to *N*-HSAH$^+$, this time with a bound water molecule (Figure 9B).

Nitrogen Protonation. By increasing the contribution of ***D*** at the expense of ***I***, N-protonation (eq 6) like O-protonation promotes nucleophilic attack at the *S*-nitroso sulfur

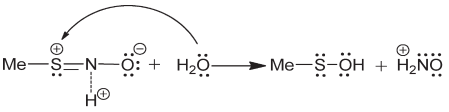

***D*H^+_N** (9)

Simultaneous S−O bond formation and proton transfer to the protonated nitrogen result in significant elongation of the S−N bond to 2.27 Å in the TS (Supporting Information, Figure S2A), which is high in energy ($\Delta H^{\ddagger}_{calc}$ is 66.2 and 56.1 kcal/mol in the gas phase and water, respectively). Although MeSOH and H_2NO^+ (or HNO at higher pH) are the products predicted by eqs 2 and 9 for attack on sulfur, the very high $\Delta H^{\ddagger}_{calc}$ indicates that this reaction is highly unlikely.

Addition of a second water molecule dramatically alters the TS (Supporting Information, Figure S2B). A proton is transferred to the *S*-nitroso oxygen, the S−N bond contracts to 1.61 Å, the TS resembles that in Figure 9B for $MeSNOH^+$, and the same *N*-HSAH$^+$ product is predicted

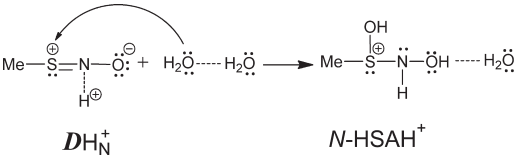

***D*H^+_N** *N*-HSAH$^+$ (10)

However, Table 3 reveals a ~10 kcal/mol increase in $\Delta H^{\ddagger}_{calc}$ for attack on the N- vs O-protonated isomer. The sulfur in the former is expected to be less electrophilic because of the

dx.doi.org/10.1021/jp1035597 |*J. Phys. Chem. B* 2011, 115, 3112–3126

significantly smaller contribution of resonance structure $\boldsymbol{D}H_N^+$ in eq 6 vs $\boldsymbol{D}H_O^+$ in eq 5. The fate of *N*-HSAH$^+$ is further considered in the Discussion.

Attack at the protonated nitrogen of MeSN(H$^+$)O was also considered

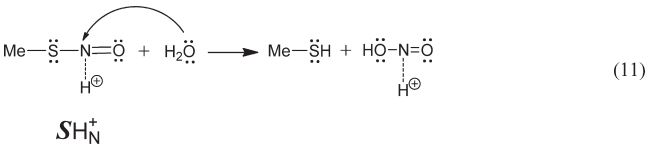

(11)

$\Delta H^{\ddagger}_{calc}$ is prohibitively large (73.5 and 59.9 kcal/mol in the gas phase and water, respectively; Supporting Information, Figure S3A) since reaction 11 requires elongation to 2.05 Å of an S−N bond that possesses significant double-bond character (eq 6). Addition of a second water molecule to assist proton transfer yields the same products, but $\Delta H^{\ddagger}_{calc}$ remains high (47.9 kcal/mol in water, Table 3).

In summary, high activation barriers (Table 3) prevent reaction occurring via the most stable *N*-protonated isomer (Figure 7A). As proposed by Williams and co-workers[12] (Scheme 1), S-protonation followed by attack at the *S*-nitroso nitrogen yielding MeSH is clearly the preferred pathway for acid-catalyzed MeSNO hydrolysis.

DISCUSSION

Experimental Trends. Williams and co-workers[12] reported that in the presence of HN_3 to trap the nitrosating agent, SNAP hydrolysis was strongly acid catalyzed with k_{obs} values of 3.21×10^{-4} and 143×10^{-4} s^{-1} in 0.94 and 4.35 M H_2SO_4, respectively. Our k_{obs} of 79.4×10^{-4} s^{-1} for SNAP hydrolysis in 3.75 M H_2SO_4 at 31 °C is in excellent agreement with their value of 81.7×10^{-4} s^{-1} in 3.77 M H_2SO_4 at the same temperature (Table 1).[12] They also reported a hydrolysis product that exhibited the same UV spectrum as the parent thiol NAP but did not quote a yield due to the product's putative instability.[12] We confirmed by HPLC analysis that the major SNAP hydrolysis product is indeed NAP (Table 2), but we found it to be stable in ∼4 M aqueous H_2SO_4 over the duration of our experiments (Figure 5G). NAP was produced in 92% yield when corrected for % reaction (Table 2), consistent with hydrolysis proceeding mainly via attack of a water molecule at the *S*-nitroso nitrogen of the S-protonated isomer RS(H$^+$)NO (eq 1 and Scheme 1) as supported by our computational results discussed below.

In addition to SNAP, we examined the acid-catalyzed hydrolysis of four other biologically and pharmacologically important RSNOs (Figure 1). CysNO, SNAC, and GSNO exhibit essentially identical k_{obs} values ($2-3 \times 10^{-4}$ s^{-1} at 31 °C) (Table 1), revealing that *N*-acylation (SNAC) and/or *N*-amidation with glycine (GSNO) (Figure 1) have negligible effects on the rate of acid-catalyzed hydrolysis of these cysteine-derived primary RSNOs. In contrast, acid hydrolysis is sensitive to dimethyl substitution at the *S*-nitroso-bearing carbon, which increased k_{obs} 12-fold (CysNO **1** vs SPEN **4**) or 34-fold (SNAC **2** vs SNAP **5**) (Table 1).

The enhanced reactivity of SNAP compared to the other RSNOs was particularly surprising given their established relative stabilities at higher pHs.[23] SNAP is routinely employed as a stable RSNO in aqueous buffers around physiological pH, whereas CysNO, for example, is highly unstable under these conditions.[23] However, the stability of RSNOs has been largely attributed to their tendency to form transient Cu^{I}−RSNO chelates with trace copper, which promotes their copper-catalyzed reductive denitrosation.[23] Under highly acidic conditions, trace copper will not successfully compete with H$^+$ for RSNO coordination, thiolate (RS$^-$)-promoted Cu^{I}/Cu^{II} redox cycling will be negligible, and Cu^{I}-catalyzed RSNO reductive decomposition will be inhibited. Thus, the variation in the k_{obs} values (Table 1) reflects the intrinsically higher reactivity of the S−N bond in tertiary vs primary RSNOs revealed by the relative energies of the $SN_{\sigma^*} \leftarrow S_{1s}$ transitions in their sulfur K-edge X-ray absorption spectra reported recently by Kennepohl and co-workers.[52]

To date, there is very limited information available on the mechanism of uncatalyzed or catalyzed RSNO hydrolysis. Our current HPLC analysis reveals that the parent RSH is present in ≥90% yield when denitrosation of both primary and tertiary RSNOs is 79−99% complete (Table 2). This observation supports a common dominant pathway for RSNO acid-catalyzed hydrolysis, which was not extended beyond 3 h (Table 2) to avoid any further reactions of the primary products. To gain mechanistic insight into the denitrosation reaction, we used quantum-chemistry calculations, selecting MeSNO as a model RSNO to decrease the computational time. The results are summarized in Table 3 for the hydrolysis reactions modeled with two water molecules. Transition states calculated for hydrolysis reactions employing only a single water molecule usually exhibit significantly higher barriers than those with two or more waters[53] (Figures 6, 8, and 9 and Supporting Information, Figures S1−S3). Thus, modeling hydrolysis reactions with one water molecule is unrealistic, whereas a "two-water-molecule" model provides a reasonable simulation of the participation of solvent molecules in hydrolysis.[54]

Uncatalyzed Hydrolysis. The experimental S−N homolytic bond dissociation energy measured at 60−80 °C in organic solvents[19] is 28.9 kcal/mol for $CH_3(CH_2)_5SNO$ and 31.6 kcal/mol for *c*-$C_6H_{11}SNO$. These values bracket the calculated S−N bond dissociation energies (∼30 kcal/mol[28]) and suggest that thermolysis is a more important RSNO decay pathway than *uncatalyzed* hydrolysis, in agreement with our computational results (Table 3) and experimental data.[12] Nonetheless, uncatalyzed hydrolysis involving nucleophilic attack at the *S*-nitroso nitrogen, which possesses a $\Delta H^{\ddagger}_{calc}$ (∼33 kcal/mol, Table 3) close to the bond dissociation energy, should compete with S−N bond homolysis in water. In contrast, attack at sulfur is unexpected since $\Delta H^{\ddagger}_{calc}$ in water is 47 kcal/mol (Table 3, Supporting Information, Figure S1). Thus, our reported observation[14] of dimedone inhibition of uncatalyzed GSNO denitrosation at 25 °C in water at pH ≈ 4 is likely due to water attack at the *S*-nitroso nitrogen (eq 1, Figure 6B) but not at the sulfur with GSOH formation (eq 2). Consistent with this proposal, we recently confirmed that, in addition to its established role as a sulfenic acid (RSOH) trap, dimedone also efficiently traps HNO_2 (Moran, E. Manuscript in preparation).

We associate the high activation enthalpies for uncatalyzed RSNO hydrolysis with the extensive elongation or contraction of the S−NO bond necessary to increase the contribution of resonance structure ***I*** or ***D*** (eq 3). However, in contrast to the weak nucleophile H_2O, the very strong nucleophile R′S$^-$ reacts rapidly with unactivated RSNOs, leading to efficient *trans*-*S*-nitrosation (RSNO + R′SH ⇌ RSH + R′SNO) around neutral pH.[23] The *S*-nitroso nitrogen is the expected target of strong

dx.doi.org/10.1021/jp1035597 |J. Phys. Chem. B 2011, 115, 3112–3126

nucleophiles since the sulfur and oxygen atoms each possess two lone pairs of electrons in the dominant resonance structure ***S*** of unactivated RSNOs (eq 3). However, GSSG and NH_3 are produced when GSNO is incubated with high [GSH],[50] indicating attack at sulfur of GSNO or another GSX species during the slow GSH-induced denitrosation of GSNO.

Acid-Catalyzed Hydrolysis. The pathways and products of acid-catalyzed RSNO hydrolysis predicted by the quantum-chemistry calculations are summarized in Figure 10. Protonation of the *S*-nitroso sulfur leads to a nascent NO^+ moiety that is highly susceptible to nucleophilic attack by water, yielding RSH, HNO_2, and H_3O^+ with a low $\Delta H^{\ddagger}_{calc}$ of ~6 kcal/mol (Table 3 and right-hand side of Figure 10). The experimental yields of ≥90% RSH on RSNOs hydrolysis (Table 2) substantiate the prominence of this denitrosation pathway in the five RSNOs examined here. NO^+ release, as evidenced by HNO_2 formation,[55] is also seen experimentally in Hg^{2+}-catalyzed RSNO decomposition,[23] which is the basis of the well-known Saville assay for RSNOs. We demonstrated computationally[17,56] that the experimentally prevailing Cu^I-catalyzed release of NO from RSNOs around neutral pH[55] arises from preferential ligation of Cu^I to the RSNO sulfur with dramatic weakening of the S−N bond. NO is released in this case presumably due to intramolecular electron transfer from Cu^I to the nascent NO^+. Hence, RSNO activation toward NO^+ release on Lewis acid coordination to the *S*-nitroso sulfur is widespread in RSNO chemistry.

Oxygen or nitrogen protonation activates the *S*-nitroso sulfur (eqs 5 and 6). Modeling of nucleophilic attack at sulfur in $MeSN(H^+)O$ with one H_2O molecule results in the sulfenic acid MeSOH and protonated HNO (eqs 2 and 9), but the activation barrier ($\Delta H^{\ddagger}_{calc} \approx 56$ kcal/mol in water, Supporting Information, Figure S2A) is prohibitively high. Addition of second water molecule to assist proton transfer lowers $\Delta H^{\ddagger}_{calc}$ to 29 kcal/mol (Table 3 and left-hand side of Figure 10), but dissociation of the *N*-$HSAH^+$ product into RSOH and protonated HNO is highly endothermic (~36 kcal/mol in water, Figure 9A). Instead, *N*-$HSAH^+$, which possesses calculated pK_a values of −9.0 (SOH^+), 2.9 (NH), and 14.0 (OH), is expected to readily lose a proton (Figure 10). N-Protonation of the resultant *N*-hydroxysufinamide, RS(=O)NHOH (Supporting Information, Figure S4A, Figure 10), which has a gas-phase proton affinity of 191.5 kcal/mol, requires 16.1 kcal/mol in water ($PA + \Delta G_{solv}$). No reaction path was found for $RS(=O)NH_2{}^+OH$ hydrolysis with two water molecules (Supporting Information, Figure S4B), but addition of four water molecules led to spontaneous nucleophilic attack of water at sulfur, giving RS(=O)OH and NH_2OH as products (Supporting Information, Figure S4B, Figure 10). Thus, acid-catalyzed RSNO hydrolysis via attack on sulfur is expected to yield the sulfinic acid RS(=O)OH and NH_2OH (or NH_3OH^+ at low pH; pK_a 6.0) and *not* the sulfenic acid RSOH and HNO as predicted by eqs 2 and 9. Since the lower barrier to *N*-$HSAH^+$ formation involves attack at sulfur of the O-protonated isomer (Table 3 and Figure 10), this is the more likely pathway to RS(=O)OH and NH_2OH production.

We speculate that RS(=O)OH is the minor product (≤10%, Table 2) of acid-catalyzed SNAP or GSNO hydrolysis. Given its greater hydrophilicity, RS(=O)OH would be retained less than the parent RSH on the reversed-phase C18 column. Thus, we predict that the peak at 6 min in the chromatogram of SNAP's hydrolysis products (Figure 5G) contains the sulfinic acid, but the high salt content (2 M Na_2SO_4) of the samples following neutralization prevented the use of LC-ESI-MS to establish the mass of this product.

Reactivity of Primary Vs Tertiary RSNOs. Although $MeS(H^+)NO$ is the least stable protonated isomer, the computational and experimental results are consistent with hydrolysis arising predominantly from attack at the *S*-nitroso nitrogen of $RS(H^+)NO$ (Tables 2 and 3). Williams and co-workers[12] correctly predicted this pathway (Scheme 1) and expressed k_{obs} at high [HN_3] as the product, K_ak_1, where k_1 is the pseudo-first-order rate constant for $RS(H^+)NO$ hydrolysis. We report a $\Delta H^{\ddagger}_{obs}$ of ~26 kcal/mol (Table 1) for the hydrolysis of SNAC, a primary RSNO, which agrees well with the sum of $\Delta H^{\circ}_{calc} + \Delta H^{\ddagger}_{calc}$ (20.7 + 6 kcal/mol) for $MeS(H^+)NO$ hydrolysis (Figure 7A, Table 3).

The tertiary RSNOs undergo acid-catalyzed hydrolysis >10-fold faster than the primary RSNOs (Table 1). To quantify the effects of the electron-donating methyl groups on the *S*-nitroso-bearing carbon in the tertiary RSNOs (Figure 1), acid dissociation constants were estimated for $MeS(H^+)NO$ and $Me_3CS(H^+)NO$. Preliminary calculations suggest a pK_a value of −16 for $MeS(H^+)NO$ and −15 for $Me_3CS(H^+)NO$. Thus, K_ak_1 for $Me_3CS(H^+)NO$ is expected to be ~10-fold greater than that for $MeS(H^+)NO$, in agreement with the order of magnitude higher k_{obs} values for acid-catalyzed hydrolysis of the tertiary vs primary RSNOs (Table 1). Notably, Williams and co-workers[12] suggested that K_a is the major determinant of the 10^6-fold faster acid-catalyzed hydrolysis of alkyl nitrites (RONOs) compared to RSNOs.

Biological Implications. Considering the very high acidity necessary to catalyze the hydrolysis of low-molecular-weight RSNOs, the physiological relevance of our results may be viewed as questionable. However, protein environments are known to dramatically alter the reactivity of various groups. For example, protein conformational change could trigger NO^+ release by bringing the *S*-nitroso sulfur in contact with a metal ion or a positively charged lysine or arginine residue and/or by activating H_2O or another nucleophile. Given its high reactivity, the fate of the nascent NO^+ would be dictated by its immediate microenvironment. Depending on the effective local pH, hydrolysis could generate HNO_2 or NO_2^-, a putative storage form of NO.[57] The nascent NO^+ could also be transferred or channeled to an adjacent thiol and protein *trans*-*S*-nitrosation is likely an important component of NO signaling in vivo.[58]

Nucleophilic attack at the *S*-nitroso sulfur is an expected minor pathway (≤10%) in acid-catalyzed hydrolysis of low molecular weight RSNOs. However, the unique environments and steric constraints imposed by protein structure could promote low-probability reactions such as attack on *S*-nitroso sulfur. Our experimental and computational results (Tables 2 and 3) predict NH_2OH, but not HNO, as a product of RSNO hydrolysis. However, hemoprotein-mediated peroxidation of NH_2OH can lead to HNO formation,[59] which may provide an indirect route for the biological synthesis of this reactive nitrogen oxide. For completeness, we note here that S−S bond formation and HNO release were observed by us[60] and others[6,60,61] for mono-*S*-nitrosated low-molecular-weight dithiols, and this is a highly likely denitrosation pathway in proteins with vicinal thiols. Since RSNO reactivity is strongly controlled by Lewis-acid coordination to the *S*-nitroso atoms, utilization of such control over protein-based *S*-nitroso groups calls for careful investigation.

CONCLUSIONS

Acid-catalyzed hydrolysis of low molecular weight primary and tertiary RSNOs produces the parent RSH in ≥90% yield. Protonation of the RSNO sulfur provides a low-energy barrier for the release of NO^+, a powerful *S*-nitrosating reagent. No low-energy pathway was found for HNO release, but a minor (≤10%) pathway is proposed that involves attack at the *S*-nitroso sulfur and yields NH_2OH and RS(=O)OH as products. The biological and pharmacological significance of RSNOs as NO^+ and NH_2OH donors, as well as RSH and RS(=O)OH donors, remains to be fully explored. Consideration of the resonance representation of RSNO electronic structure (eq 3) was central in our computational analysis of RSNO hydrolysis and will be key in deciphering the reactivity of the SNO group in proteins.

ASSOCIATED CONTENT

Supporting Information. Modeling of hydrolysis: uncatalyzed attack at the sulfur of MeSNO (Figure S1), attack at the sulfur of N-protonated MeSNO (Figure S2), attack at nitrogen of N-protonated MeSNO (Figure S3), and structures of N-protonated *N*-hydroxysufinamide and its complexes with water molecules (Figure S4); Cartesian coordinates are provided for the calculated molecules and transition states. This material is available free of charge via the Internet at http://pubs.acs.org.

AUTHOR INFORMATION

Corresponding Authors

*E-mail: english@alcor.concordia.ca, qadir.timerghazin@mu.edu.

Present Addresses

[§]Current address: Department of Chemistry, Marquette University, Milwaukee, WI 53201.

ACKNOWLEDGMENT

This work was funded by grants from the Natural Sciences and Engineering Research Council (NSERC) of Canada, the Canadian Institutes of Health Research (CIHR), and Merck Frosst Canada Inc. to A.M.E. Calculations were performed within the Réseau québécois de calcul haute performance (RQCHP) and at the Centre for Research in Molecular Modeling (CERMM), which was established with financial support from the Faculty of Arts and Science, Concordia University, the Ministère de l'Éducation du Québec, and the Canada Foundation for Innovation. E.E.M. acknowledges graduate student support from Merck Frosst Canada Inc., Q.K.T. was supported by a NSERC Postdoctoral Fellowship, and A.M.E. holds a Concordia University Research Chair. The authors wish to thank Elena Ivanova (Concordia University) for useful suggestions regarding the transition-state calculations.

REFERENCES

(1) Knowles, R. G.; Moncada, S. *Biochem. J.* **1994**, *298*, 249.
(2) Moncada, S.; Palmer, R. M.; Higgs, E. A. *Pharmacol. Rev.* **1991**, *43*, 109.
(3) Fukuto, J. M.; Switzer, C. H.; Miranda, K. M.; Wink, D. A. *Annu. Rev. Pharmacol. Toxicol.* **2005**, *45*, 335.
(4) Hogg, N. *Free Radical Biol. Med.* **2000**, *28*, 1478.
(5) Stamler, J. S.; Toone, E. J. *Curr. Opin. Chem. Biol.* **2002**, *6*, 779.
(6) Arnelle, D. R.; Stamler, J. S. *Arch. Biochem. Biophys.* **1995**, *318*, 279.
(7) Stamler, J. S.; Singel, D.; Loscalzo, J. *Science* **1992**, *258*, 1898.
(8) Girard, P.; Potier, P. *FEBS Lett.* **1993**, *320*, 7.
(9) Jia, L.; Bonaventura, C.; Bonaventura, J.; Stamler, J. S. *Nature* **1996**, *380*, 221.
(10) Miranda, K. M.; Paolocci, N.; Katori, T.; Thomas, D. D.; Ford, E.; Bartberger, M. D.; Espey, M. G.; Kass, D. A.; Feelisch, M.; Fukuto, J. M.; Wink, D. A. *Proc. Natl. Acad. Sci. U.S.A.* **2003**, *100*, 9196.
(11) *The Merck Index*, 12th ed.; Merck & Co, Inc.: Whitehouse Station, NJ, 1996.
(12) Al-Kaabi, S. S.; Williams, D. L. H.; Bonnet, R.; Ooi, S. L. *J. Chem. Soc., Perkin Trans. 2* **1982**, 227.
(13) Mathews, A. P.; Walker, S. *J. Biol. Chem.* **1906**, *6*, 21.
(14) Tao, L.; English, A. M. *Biochemistry* **2004**, *43*, 4028.
(15) Davis, F. A. *J. Org. Chem.* **2006**, *71*, 8993.
(16) Davis, F. A.; Jenkins, L. A.; Billmers, R. L. *J. Org. Chem.* **1986**, *51*, 1033.
(17) Timerghazin, Q. K.; Peslherbe, G. H.; English, A. M. *Org. Lett.* **2007**, *9*, 3049.
(18) Weinhold, F.; Landis, C. R. *Valency and Bonding: A Natural Bond Orbital Donor-Acceptor Perspective*; Cambridge University Press: Cambridge, U.K., 2005.
(19) Bartberger, M. D.; Houk, K. N.; Powell, S. C.; Mannion, J. D.; Lo, K. Y.; Stamler, J. S.; Toone, E. J. *J. Am. Chem. Soc.* **2000**, *122*, 5889.
(20) Baciu, C.; Gauld, J. W. *J. Phys. Chem. A* **2003**, *107*, 9946.
(21) Hart, T. W. *Tetrahedron Lett.* **1985**, *26*, 2013.
(22) Williams, D. L. H. *Nitrosation reactions and the chemistry of nitric oxide*; Elsevier: New York, 2004.
(23) Williams, D. L. H. *Acc. Chem. Res.* **1999**, *32*, 869.
(24) Montgomery, J. A., Jr.; Frisch, M. J.; Ochterski, J. W.; Petersson, G. A. *J. Chem. Phys.* **1999**, *110*, 2822.
(25) Montgomery, J. A., Jr.; Frisch, M. J.; Ochterski, J. W.; Petersson, G. A. *J. Chem. Phys.* **2000**, *112*, 6532.
(26) Ochterski, J. W.; Petersson, G. A.; J. A. Montgomery, J. *J. Chem. Phys.* **1996**, *104*, 2598.
(27) Frisch, M. J.; Trucks, G. W.; Schlegel, H. B.; Scuseria, G. E.; Robb, M. A.; Cheeseman, J. R.; Montgomery, J. A., Jr.; Vreven, T. J.; Kudin, K. N.; Burant, J. C.; Millam, J. M.; Iyengar, S. S.; Tomasi, J.; Barone, V.; Mennucci, B.; Cossi, M.; Scalmani, G.; Rega, N.; Petersson, G. A.; Nakatsuji, H.; Hada, M.; Ehara, M.; Toyota, K.; Fukuda, R.; Hasegawa, J.; Ishida, M.; Nakajima, T.; Honda, Y.; Kitao, O.; Nakai, H.; Klene, M.; Li, X.; Knox, J. E.; Hratchian, H. P.; Cross, J. B.; Bakken, V.; Adamo, C.; Jaramillo, J.; Gomperts, R.; Stratmann, R. E.; Yazyev, O.; Austin, A. J.; Cammi, R.; Pomelli, C.; Ochterski, J. W.; Ayala, P. Y.; Morokuma, K.; Voth, G. A.; Salvador, P.; Dannenberg, J. J.; Zakrzewski, V. G.; Dapprich, S.; Daniels, A. D.; Strain, M. C.; Farkas, O.; Malick, D. K.; Rabuck, A. D.; Raghavachari, K.; Foresman, J. B.; Ortiz, J. V.; Cui, Q.; Baboul, A. G.; Clifford, S.; Cioslowski, J.; Stefanov, B. B.; Liu, G.; Liashenko, A.; Piskorz, P.; Komaromi, I.; Martin, R. L.; Fox, D. J.; Keith, T.; Al-Laham, M. A.; Peng, C. Y.; Nanayakkara, A.; Challacombe, M.; Gill, P. M. W.; Johnson, B.; Chen, W.; Wong, M. W.; Gonzalez, C.; Pople, J. A. *Gaussian 03*, Revision B.05; Gaussian Inc.: Pittsburgh, PA, 2003.
(28) Timerghazin, Q. K.; Peslherbe, G. H.; English, A. M. *Phys. Chem. Chem. Phys.* **2008**, *10*, 1532.
(29) Timerghazin, Q. K.; English, A. M.; Peslherbe, G. H. *Chem. Phys. Lett.* **2008**, *454*, 24.
(30) Stephens, P. J.; Devlin, F. J.; Chabalowski, C. F.; Frisch, M. J. *J. Phys. Chem.* **1994**, *98*, 11623.
(31) Becke, A. D. *J. Chem. Phys.* **1996**, *104*, 1040.
(32) Lee, C.; Yang, W.; Parr, R. G. *Phys. Rev. B: Condens. Matter Mater. Phys.* **1988**, *37*, 785.
(33) Nyden, M. R.; Petersson, G. A. *J. Chem. Phys.* **1981**, *75*, 1843.
(34) Houk, K. N.; Hietbrink, B. N.; Bartberger, M. D.; McCarren, P. R.; Choi, B. Y.; Voyksner, R. D.; Stamler, J. S.; Toone, E. J. *J. Am. Chem. Soc.* **2003**, *125*, 6972.
(35) Zhao, Y.-L.; McCarren, P. R.; Houk, K. N.; Choi, B. Y.; Toone, E. J. *J. Am. Chem. Soc.* **2005**, *127*, 10917.

(36) Cossi, M.; Rega, N.; Scalmani, G.; Barone, V. *J. Comput. Chem.* **2003**, *24*, 669.
(37) Cossi, M.; Scalmani, G.; Rega, N.; Barone, V. *J. Chem. Phys.* **2002**, *117*, 43.
(38) Tissandier, M. D.; Cowen, K. A.; Feng, W. Y.; Gundlach, E.; Cohen, M. H.; Earhart, A. D.; Coe, J. V.; Tuttle, T. R. *J. Phys. Chem. A* **1998**, *102*, 7787.
(39) Camaioni, D. M.; Schwerdtfeger, C. A. *J. Phys. Chem. A* **2005**, *109*, 10795.
(40) Li, J.; Wang, G. P.; Schlegel, H. B. *Org. Biomol. Chem.* **2006**, *4*, 1352.
(41) Verdolino, V.; Cammi, R.; Munk, B. H.; Schlegel, H. B. *J. Phys. Chem. B* **2008**, *112*, 16860.
(42) Cances, E.; Mennucci, B.; Tomasi, J. *J. Chem. Phys.* **1997**, *107*, 3032.
(43) Fukui, K. *Acc. Chem. Res.* **2002**, *14*, 363.
(44) Jensen, F. *J. Chem. Phys.* **2002**, *117*, 9234.
(45) Perdew, J. P.; Burke, K.; Ernzerhof, M. *Phys. Rev. Lett.* **1996**, *77*, 3865.
(46) Stedman, G. *J. Chem. Soc.* **1959**, 2943.
(47) Chipinda, I.; Simoyi, R. H. *J. Phys. Chem. B* **2006**, *110*, 5052.
(48) Goldstein, S.; Czapski, G. *Inorg. Chem.* **1996**, *35*, 7735.
(49) Davis, F. A.; Billmers, R. L. *J. Am. Chem. Soc.* **1981**, *103*, 7016.
(50) Wong, P. S. Y.; Hyun, J.; Fukuto, J. M.; Shirota, F. N.; DeMaster, E. G.; Shoeman, D. W.; Nagasawa, H. T. *Biochemistry* **1998**, *37*, 5362.
(51) Hunter, E. P.; Lias, S. G. *J. Phys. Chem. Ref. Data* **1998**, *27*, 413.
(52) Martin-Diaconescu, V.; Perepichka, I.; Bohle, D. S.; Kennepohl, P. *Can. J. Chem.* **2011**, in press.
(53) Wu, Z.; Ban, F.; Boyd, R. J. *J. Am. Chem. Soc.* **2003**, *125*, 6994.
(54) Ivanova, E. V.; Muchall, H. M. *J. Phys. Chem. A* **2007**, *111*, 10824.
(55) Swift, H. R.; Williams, D. L. H. *J. Chem. Soc., Perkin Trans. 2* **1997**, 1933.
(56) Toubin, C.; Yeung, D. Y.-H.; English, A. M.; Peslherbe, G. H. *J. Am. Chem. Soc.* **2002**, *124*, 14816.
(57) Gladwin, M. T.; Raat, N. J. H.; Shiva, S.; Dezfulian, C.; Hogg, N.; Kim-Shapiro, D. B.; Patel, R. P. *Am. J. Physiol. Heart Circ. Physiol.* **2006**, *291*, H2026.
(58) Hess, D. T.; Matsumoto, A.; Kim, S.-O.; Marshall, H. E.; Stamler, J. S. *Nat. Rev. Mol. Cell Biol.* **2005**, *6*, 150.
(59) Donzelli, S.; Espey, M. G.; Flores-Santana, W.; Switzer, C. H.; Yeh, G. C.; Huang, J.; Stuehr, D. J.; King, S. B.; Miranda, K. M.; Wink, D. A. *Free Radical Biol. Med.* **2008**, *45*, 578.
(60) Roy, J.-F.; Chrétien, M. N.; Woodside, B.; English, A. M. *Nitric Oxide* **2007**, *17*, 82.
(61) Stoyanovsky, D. A.; Tyurina, Y. Y.; Tyurin, V. A.; Anand, D.; Mandavia, D. N.; Gius, D.; Ivanova, J.; Pitt, B.; Billiar, T. R.; Kagan, V. E. *J. Am. Chem. Soc.* **2005**, *127*, 15815.